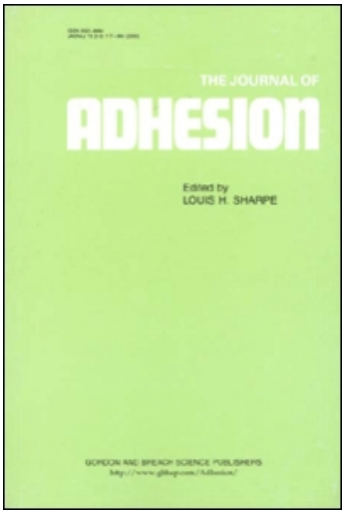

The Journal of Adhesion
Publication details, including instructions for authors and subscription information:
http://www.informaworld.com/smpp/title~content=t713453635

Experimental Investigation of the Interphase in an Epoxy-Aluminum System

V. Safavi-Ardebili[a]; A. N. Sinclair[a]; J. K. Spelt[a]
[a] Department of Mechanical & Industrial Engineering, University of Toronto, Toronto, Ontario, Canada

To cite this Article Safavi-Ardebili, V. , Sinclair, A. N. and Spelt, J. K.(1997) 'Experimental Investigation of the Interphase in an Epoxy-Aluminum System', The Journal of Adhesion, 62: 1, 93 — 111
To link to this Article: DOI: 10.1080/00218469708014564
URL: http://dx.doi.org/10.1080/00218469708014564

J. Adhesion, 1997, Vol. 62, pp. 93–111
Reprints available directly from the publisher
Photocopying permitted by license only

Experimental Investigation of the Interphase in an Epoxy-Aluminum System

V. SAFAVI-ARDEBILI, A. N. SINCLAIR and J. K. SPELT*

Department of Mechanical & Industrial Engineering, University of Toronto, 5 King's College Road, Toronto, Ontario, Canada M5S 3G8

(Received 2 July 1996; In final form 14 November 1996)

The interphase in an epoxy-aluminum system has been revealed and characterized using scanning electron microscopy, ion etching, energy-dispersive x-ray analysis, and nano-indentation. The interphase was of irregular thickness, nominally between 2 and 6 μm, and corresponds to a region of greater resistance to ion etching and a marked absence of the silica particles used in the epoxy adhesive. Nano-indentation tests, traversing various sections of the interphase from the aluminum to the bulk resin, showed that the interphase region had, on average, an effective elastic modulus ($E/(1-\nu^2)$) that was 13% greater than that of the bulk resin, far from the aluminum. The interphase was also approximately 4% harder than the bulk adhesive.

Keywords: Interphase (thickness, modulus, structure); mechanical properties; epoxy adhesive; SEM; ion etching; EDX; nano-indentation

INTRODUCTION

It is commonly believed that, in the interfacial region between a polymer and a solid substrate, a layer of polymer can be distinguished which has different properties from that of the bulk polymer. This "interphase" has been the subject of much interest in recent years because of its likely role in determining the mechanical properties and durability of adhesive joints, and matrix-fiber bonds in composite materials. The present paper examines the extent and mechanical properties of the interphase between

*Corresponding author.

an epoxy adhesive and an aluminium adherend. The work formed part of an ongoing effort to use ultrasonic nondestructive evaluation as a means of monitoring environmental degradation in adhesive joints. Multilayer sound wave propagation models applied to adhesive joints require estimates of the interphase elastic constants.

Cuthrell [1] found that several unfilled (without inorganic particles), untoughened (not containing rubber particles) epoxy resins displayed an interphase consisting of "floccules" of polymer surrounded by resin of different structure. Chemical etching and indentation tests showed that the floccules were harder and more rigid than the surrounding epoxy, and that their size was a function of the initial rate of cure. These interfacial regions could extend from the adherend several hundred micrometers into the bulk resin.

Hahn and Koetting [2] used ion etching and scanning electron microscopy to reveal the interphase in systems of expoxy-aluminum and phenolic-aluminum. Close to the aluminum, both adhesives had a lamellar structure oriented perpendicular to the metal surface, while the bulk resins had a globular morphology. There was an irregular boundary between these morphologies. As with Cuthrell [1], the chemical nature of the metal surface affected the morphology; Hahn and Koetting [2] did not find the lamellar structure when the aluminum surface was contaminated, as it was in the "as received" condition.

The variation of shear modulus, G, through the interphase has been measured by Knollman [3] in an epoxy-aluminum systems using ultrasonic Rayleigh waves. G increased from 1.9 to 2.5 GPa as distance from the aluminum increased from 0.1 to 0.4 mm. The extent of the interphase was increased by longer epoxy cure times. Williams *et al.* [4] also observed a softer interphase in fiber pull-out experiments with epoxy resin and carbon fibers that were either oxidized or coated with an adhesion-promoting commercial size. When carbon fibers were coated with ε phenolic resin, the interphase was absent. Crompton [5] used transmission electron microscopy of ultramicrotomed sections cut normal to the interface to reveal two types of interphase in an epoxy-aluminum system. Changes in electron transparency occured over a distance of approximately 1 μm from the aluminum, and often contained a second distinctive region formed in the first 10 nm of resin adjacent to the interface. The boundary between the interphase and the bulk resin was highly irregular. The interphase seemed to contain, on average, less fumed

silica than the bulk, although a more pronounced characteristic was associated with differences in the polymer structure between the bulk and the interphase. These observations were unaffected by the aluminum pretreatment, which was either an acid etch or a chemical conversion coat.

Using single filament fragmentation tests as a function of temperature, Skourlis and McCullough [6] found that the critical aspect ratio of fragments reflected an interphase having a glass transition temperature less then that of the bulk resin.

Cognard [7] used scanning acoustic microscopy to reveal a honeycomb-like interfacial structure parallel to the interface of an epoxy-gold system. The average cell diameter was approximately 15–30 μm, and the interphase was estimated to extend 3–4 μm from the gold surface into the epoxy.

Maguire *et al.* [8] have discussed the origin of the interphase and its thickness, which ranges several orders of magnitude, *i.e.* a few Angstroms up to several micrometers. They have reviewed the molecular dynamic simulations and related studies, and demonstrated the possibility of the formation of a thick interphase (of the thickness in the micrometer range) by introducing non-linearity in their model calculations.

One possible explanation for the difference between the polymer structure in the bulk and the interphase of epoxy-aluminum systems is a localization of the curing agent at the aluminum interface. Using X-ray photoelectron spectroscopy and Fourier transform infra-red spectroscopy, Nakamae *et al.* [9] found that 4,4′-diaminodiphenylmethane (DDM) adsorbed preferentially onto aluminum oxide. Similar observations have been made by Affrosman *et al.* [10].

Using high surface area carbon black as the model surface, Wang and Garton [11] showed the importance of the interfacial reactions for difunctional epoxy resins cured with either anhydrides or aromatic amines. Adsorption and catalytic effects produced an interphase with reduced cross-link density.

EXPERIMENTS

The interphase under investigation was that associated with FPL-etched [12] aluminum alloy Al-1100 bonded with the single-part paste

epoxy, Hysol EA-9346. This adhesive contains 1 to 5% (by weight) hydrophobic SiO_2 particles. Prior to the FPL etch, the aluminum was polished using a sequence of abrasive papers of up to 600 mesh, then using 5 μm polycrystalline diamond suspension on a hard pad to retain flatness. Next, a 1 μm polycrystalline diamond suspension was used on a soft pad, followed by a 0.05 μm alumina suspension.

After the aluminum had been pretreated it was warmed to between 40°C and 50°C to ease the spreading of the adhesive and reduce the incidence of voids. Bondline thickness was controlled at 0.4 mm using Teflon shims, and the adhesive was cured nominally at 120°C for one hour; Figure 1 shows the temperature-time history of a typical joint, recorded with a thermocouple embedded in the adhesive bondline.

Four types of specimens were prepared, as shown in Figure 2. A typical joint had lateral dimensions of 2.5 × 5 cm. Types N and O were prepared using an abrasive disk cutter, with aluminum alloy 7075-T6 used as a second adherend for ease of handling. The interphase of type N specimens was examined in a plane perpendicular to the aluminum surface, while that of type O specimens was exposed at an angle of 6° from the plane of the aluminum surface. This effectively magnified the linear extent of the interphase by a factor of ten. Type P and M specimens were prepared with an ultramicrotome; type P being cut parallel to the 1100 alloy surface, type M cut at an angle less than 6° to the original surface of the 1100 alloy. Type N and O specimens were polished using the same procedure described above for polishing the aluminum substrates, always taking great care to prevent the formation of relief at the adhesive-aluminum interface.

The interfacial regions of type N and O specimens were etched using an argon ion mill, nominally operating at 4 kV with an ion

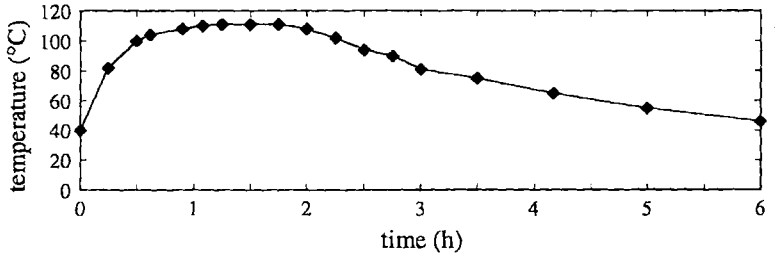

FIGURE 1 Cure cycle for the EA9346 adhesive as measured with a thermocouple embedded in the bondline.

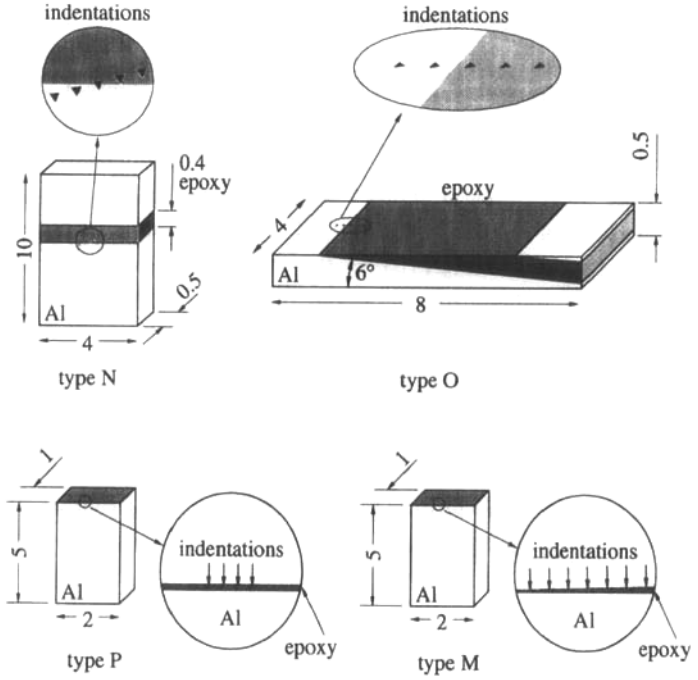

FIGURE 2 The four types of specimens with their dimensions (mm), showing the orientations of each series of nano-indentations.

current of 0.1 mA. Cleaning was achieved at an angle of 10° relative to the surface for 20 s, and etching at 35° for 200 s.

The interphase of type O specimens was examined using energy-dispersive x-ray analysis (EDX) to obtain spatial maps of the elements C, Si and Al.

Nano-indentation tests were performed on all types of specimens using a custom-built instrument at the Kingston Research and Development Centre of Alcan International Ltd. The device used a Berkovitch 3-sided pyramidal indenter, and had depth and force resolutions of 0.4 nm and less than 20 μN, respectively. The loading and unloading were performed under displacement control at 20 nm/s. The maximum depth of indentation was approximately 200 nm, and zero dwell time at the maximum load was used to reduce creep effects. For each indentation, loading-unloading curves of the types shown in Figure 3a were obtained. To reduce the effect of noise, both the load

and depth data arrays were smoothed using a boxcar filter of 13 points, as shown in Figure 3b.

Using the method of Oliver and Pharr [13], the contact stiffness and the depth of indentation were calculated from the unloading data. The reduced modulus ($E_r = E/(1-\nu^2)$) was then calculated taking into account the effect of the aluminum substrate using the empirical relation suggested by Doerner and Nix [14] with the theoretically determined parameters of King [15]. In the Oliver and Pharr method for the analysis of indentation data, the unloading curve (load *versus* depth) is fitted to a power law relationship,

$$P = \delta (h - h_f)^m \tag{1}$$

where P is the load, h is the indentation depth, and h_f is the depth at which the indenter load returns to zero upon unloading (plastic deformation produces some hysteresis). The values of δ, m and h_f, are

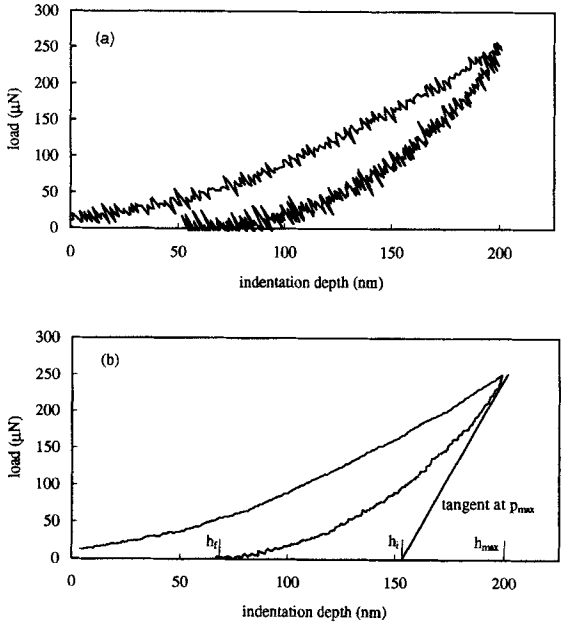

FIGURE 3 Load *vs.* depth of indentation, loading and unloading curves: a. Unfiltered data; b. Filtered data, showing definitions of parameters h_f, h_i and h_{max}.

obtained by first correcting the indentation depths, h, for the error introduced by finite machine compliance, and then fitting the load-depth data to Eq. (1). As suggested in [16], only the portion of the unloading curve between 40% and 90% of the maximum load was used in the curve fitting. This reduces the effect of creep during unloading, and minimizes errors due to uncertainties in the description of the indenter geometry; errors which are greatest near the tip. The next step was to calculate the contact depth, h_c, as

$$h_c = h_{\max} - \varepsilon(h_{\max} - h_i) \tag{2}$$

where $h_{\max}$ is the depth at maximum load and h_i is the depth corresponding to the intersection of the depth axis (at zero load) and the tangent to the fitted unloading curve at the point of maximum load (Fig. 3b). The factor ε is taken equal to 0.75 following the reference [13]'s line of reasoning. The contact depth is the distance between the tip of the indenter and the plane where the surface of the specimen departs from the faces of the indenter. The contact unloading stiffness at maximum load, dP/dh, is the slope of the tangent line to the power law fitted curve. This stiffness value was used to obtain an uncorrected reduced modulus, E_{ru}, using

$$dP/dh = \beta E_{ru}\sqrt{A} \tag{3}$$

where β has a theoretically determined value of 1.167 [15], and A is the cross-sectional area of the indenter as a function of distance from the indenter tip. Finally, E_{ru} was corrected for the effects of diamond indenter and aluminum substrate elasticity to yield to reduced modulus of the adhesive, E_r, using the relation

$$\frac{1}{E_{ru}} = \frac{1}{E_r}(1 - e^{-\alpha t/a}) + \frac{1}{E_{rs}}e^{-\alpha t/a} + \frac{1}{E_{ri}} \tag{4}$$

where E_{rs} and E_{ri} are, respectively, the modulus of the aluminum substrate and the indenter, a is the square root of the indenter cross-sectional area, A, at maximum load, t is the thickness of the epoxy at the indentation site, and α is a function of a/t as given in Ref. [15].

RESULTS

Figure 4 shows scanning electron micrographs of the interfacial region of an O-type specimen. Because the interphase was exposed at an angle of 6°, the effective magnification of distances perpendicular to the interface is 10 times greater than that indicated by the SEM; *i.e.* 10 μm on the photograph in the direction perpendicular to the scale bar (or interface) represents 1 μm normal to the aluminum interface. Figures 4a, b and c show the highly polished adhesive in the interfacial region after ion etching, at progressively higher magnifications. The irregular adhesive-aluminum boundary is at the bottom of each figure. There is a distinct difference in the morphology of the bulk

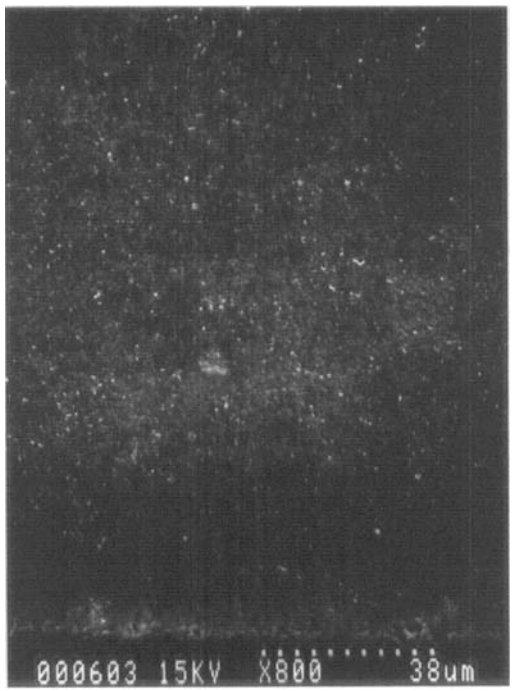

(a)

FIGURE 4 Scanning electron micrographs of the aluminum-epoxy interfacial region of an O-type specimen; a,b,c. Increasing magnifications of the same area after polishing and ion etching; aluminum-adhesive boundary is seen near the bottom of each photograph. d. High magnification view of bulk adhesive after polishing and ion etching; e. High magnification view of bulk adhesive after polishing but before ion etching.

(b)

FIGURE 4 (Continued).

adhesive and the region near the aluminum (within approximately 20 μm of the aluminum on Fig. 4b, corresponding to within 2 μm normal to the interface). The bulk adhesive appears to be rougher, with move voids. Comparison of Figures 4d and 4e, high magnification views of the bulk adhesive after and before ion etching, respectively, shows that this morphology difference is due to the ion etching. Comparing Figures 4c and 4d, high magnification images after ion etching of the interfacial region and the bulk, respectively, suggests that the interphase is more resistant to the ion etching than the bulk since the interphase is smoother. Similar features were observed in type N specimens.

Energy-dispersive x-ray maps of carbon and silicon for an O-type specimen after ion milling are shown in Figures 5a and 5b, respectively. Figures 5c shows the superposition of Figures 5a and 5b along with the Al which is shown in blue. As with Figure 4, since these

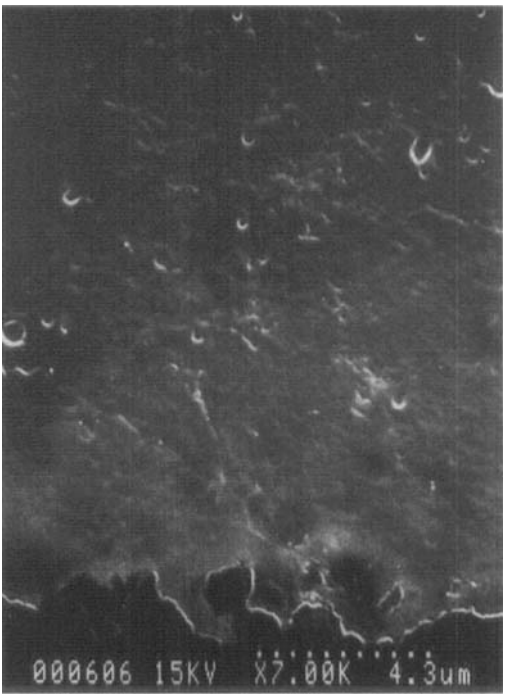

(c)

FIGURE 4 (Continued).

micrographs are of a 6° tapered surface, the effective magnification of the interphase is 10 times greater than indicated by the scale bar. The carbon map shows the extent of the adhesive with the blue arrows at the bottom of the figure indicating the boundary with the bare aluminum. Comparison of the carbon and silicon maps reveals that the interphase has very much less silicon than does the bulk adhesive; in fact, no silicon was detected in this region (the small silicon signal evident in the interphase is background noise). This suggests that the SiO_2 filler particles are segregating during the application and cure of the adhesive. The extent of the interphase, as defined by the silicon-depleted zone, is indicated by the blue arrows in Figure 5b; in this case it is just over 30 μm in width (3 μm normal to the interface).

Figure 4d shows the bulk epoxy after ion etching. It is possible that the observed pits are the result of a preferential etching of a softer polymer surrounding silica particles. The interphase, shown in Figure 4c, being

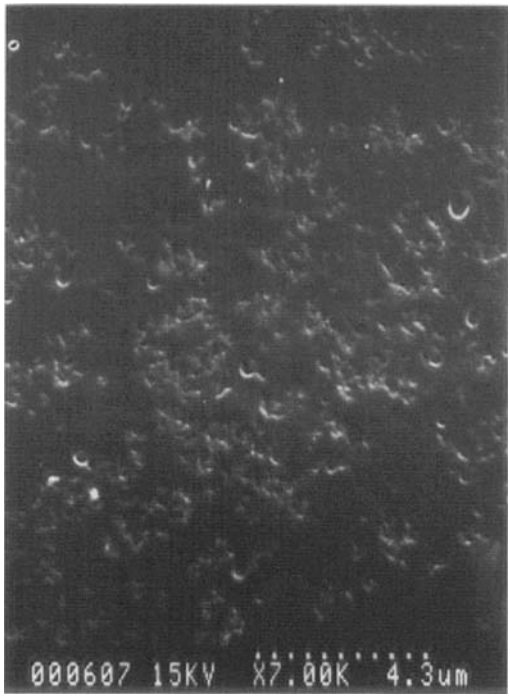

(d)

FIGURE 4 (Continued).

relatively free of silica, does not become similarly pitted by the ion etching. It is very unlikely that the pits reflect the removal of silica; since silicon is heavier than carbon it would not be preferentially etched. Moreover, the density of the pits on the surface is much greater than what would be expected from the amount of silica present in the adhesive; *i.e.* 1%–5% silica by weight would mean only 0.5%–2.5% silica by volume.

Figure 6 shows the reduced modulus of the adhesive, E_r, *versus* the perpendicular distance from the aluminum for nano-indentation measurements done on five O-type, five P-type and one M-type specimen. The results were similar for these types of specimens, indicating that preparation methods (polished or microtomed surfaces) were not influencing the data. A comparison of data for $t = 20\,\mu m$ between O-type and P-type showed a 1% difference with no statistical significance. Each data point on the graph represents the average of 25 indentations from a total of more than 400 indentations, each with a

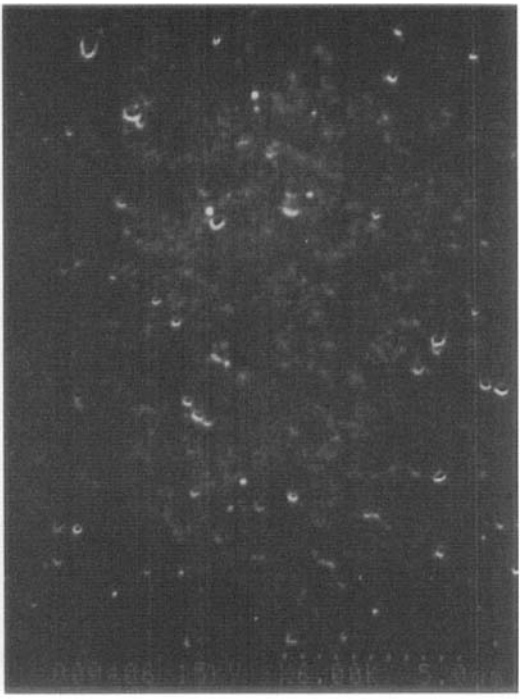

(e)

FIGURE 4 (Continued).

maximum depth between 170 and 230 nm. Data are not shown for measurements corresponding to distances less than 1 μm normal to the aluminum interface because of the possibility that the underlying aluminum affects the tests on such thin layers. Error bars on each point show the thickness span and the spread in E_r values in terms of one standard deviation. As the distance normal to the interface decreases from 70 μm to 1 μm, the reduced modulus increases such that the average E_r for the interphase (distance normal to the interface, t, between 1 μm and 5 μm) is 13% greater than the average in the bulk ($t > 20$ μm) with a significance level of more than 99.9% (t test); specifically, 3.65 GPa in the interphase and 3.22 GPa in the bulk. The same data, when interpreted for Berkovitch hardness, show that the interphase (defined here as between 1 μm–5 μm normal to the aluminum interface) is 4.2% harder than the bulk adhesive (0.275 GPa compared with 0.263 GPa) with a significance of 95% (t test).

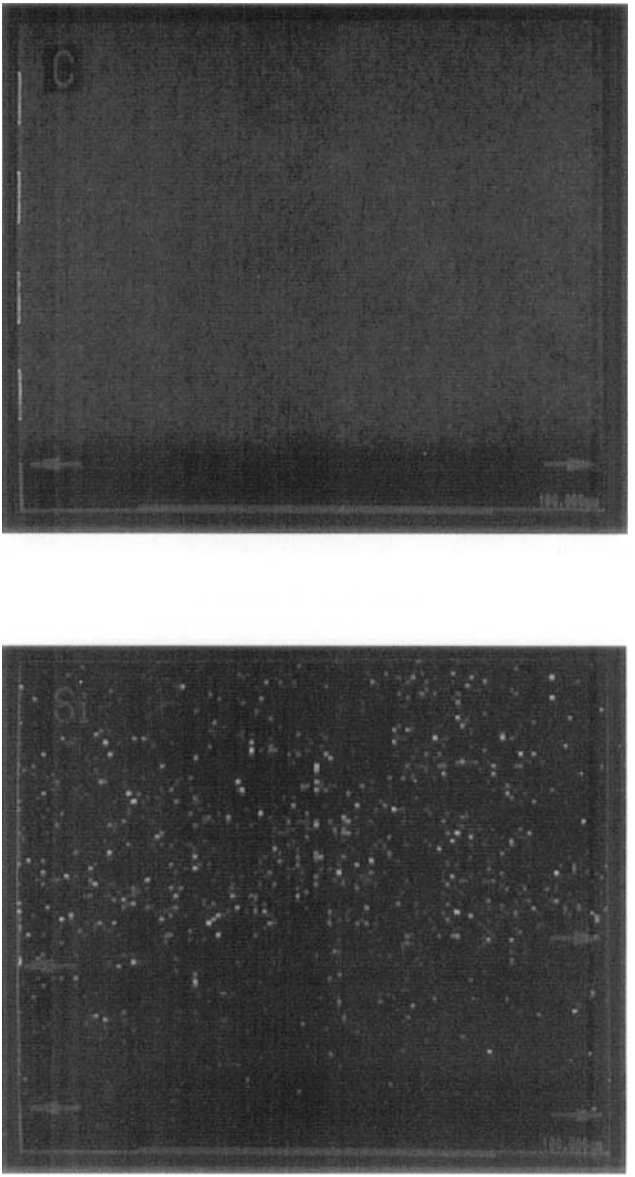

(a)

(b)

FIGURE 5 Energy-dispersive x-ray maps of the interfacial region of an ion-etched O-type specimen at a taper-angle of 6°: a. Carbon (violet). Arrows indicate approximate aluminum interface; b. Silicon (yellow). Lower arrows indicate aluminum interface, upper arrows indicate approximate extent of silicon-depleted zone; c. Superposition of carbon and silicon maps with aluminum shown in blue. (See Color Plate I).

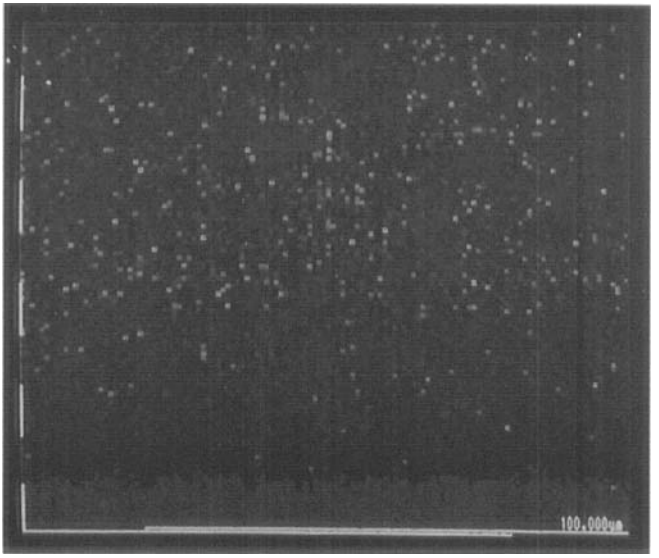

FIGURE 5 (Continued).

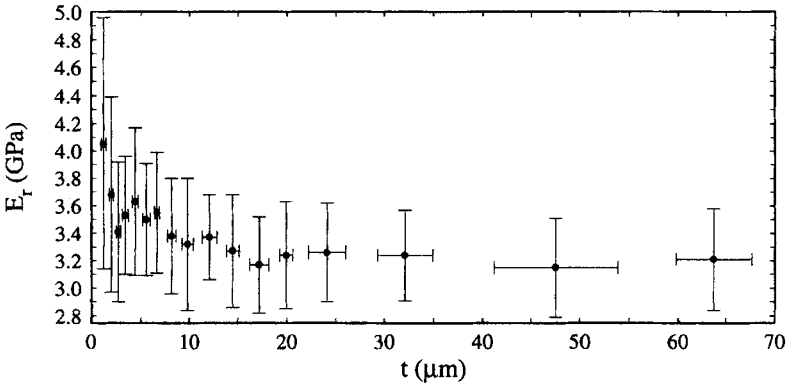

FIGURE 6 Reduced modulus, E_r, *vs.* thickness of remaining adhesive layer, t, as calculated from nano-indentation data on O, P and M-type specimens.

Figure 7 shows nano-indentation results on a single type-N specimen. Because the lateral size of the indentation is comparable with the distance normal to the aluminum, t, the effect of the aluminum may influence the measurement for a greater depth into the adhesive.

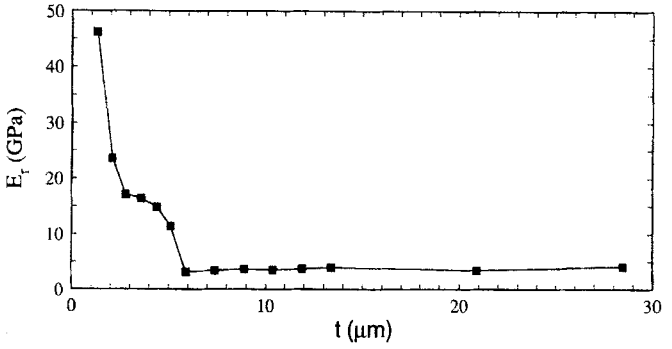

FIGURE 7 Reduced modulus, E_r, *vs.* thickness of remaining adhesive layer, t, as calculated from nano-indentation data on an N-type specimen.

Nevertheless, for this case, the E_r values were not corrected for the presence of the relatively stiff aluminum half-space in the lateral direction, as there is no theory available to do this.

DISCUSSION

The nano-indentation results of Figures 6 and 7 indicate that the interphase is harder and has a greater reduced modulus of elasticity than does the bulk adhesive. This is consistent with the scanning electron micrographs of Figure 4, which show that the interphase is more resistant to the creation of surface roughness by argon ion etching. It is also consistent with the observations of Cuthrell [1].

Figure 4 also reveals that the interphase boundary in this system is highly irregular, similar to the observations of Hahn and Koetting [2] and Crompton [5]. It is, therefore, to be expected that polished tapered sections through the interphase will produce a patch-wise heterogeneous structure, resulting in considerable variation in nano-indentation data across such a region.

One of the sources of error in nano-indentation testing is the determination of the point at which the tip of the pyramidal indenter contacts the surface. This uncertainity has been demonstrated to be one of the causes of the "indentation size effect" [17]. To reduce this error, the location of the zero-load point at the start of loading was

estimated by fitting a straight line to the load-indentation data points between 2 and 15% of the maximum load of the test. All indentation depths were then shifted so that zero load occurred at zero indentation. This resulted in various total depths of indentation for individuals tests, as opposed to a constant intended depth of 200 nm. Only indentations with a maximum depth of between 170 and 230 nm were then used to obtain the modulus.

Nano-indentation tests can be complicated by a varying and uncertain machine compliance, and by uncertainity in the indenter-tip area function [16]. It has been shown [18] that the latter is well-approximated by a pyramid shape having a truncated tip. In the present analysis, the average machine compliance and the tip truncation length were estimated using data obtained on bare aluminum. The difference between the average calculated modulus of aluminum and the literature value (69 GPa) was minimized by taking the machine compliance and the tip truncation length as optimization parameters. These parameters were then used in the load-depth analysis procedures to correct the depth data and calculate the tip area function, respectively.

The apparent modulus and hardness of the adhesive can be affected by the proximity of the underlying aluminum substrate. It is commonly believed, however, that the measurement of hardness is unaffected by a relatively hard substrate if the indentation depth is less than 1/4 of the thickness of the soft layer [19]. In fact, it has been shown that the indentation depth can equal the coating thickness in cases where the coating is extremely soft compared with the substrate [20]. In the present experiments, the indentation depth was always less than 1/4 of the thickness of the remaining adhesive layer on tapered specimens.

With respect to the measurement of Young's modulus, there is greater uncertainity as to the effect of the substrate. For the case of epoxy on aluminum, Eq. (4) reveals that the effect of the substrate on the modulus becomes negligible only when the indentation depth is less than 1/15th of the epoxy layer thickness. This is why Eq. (4) was used to correct the modulus in the present data analysis.

The present observation of silicon depletion in the interphase (Fig. 5) is similar to that made by Crompton [5]. It is possible that this phenomenon may be related to the fact that hydrophobic silica particles would be rejected by the advancing solid phase of an epoxy resin

that begins crosslinking preferentially from the aluminum surface. Recall that earlier experimental work on other epoxies has shown that curing agents can adsorb preferentially on to the aluminum [9, 10], thereby possibly causing a local acceleration of crosslinking. The fate of hydrophobic silica particles can be predicted by an analysis of the change in the Helmholtz free energy of adhesion, ΔF^{adh}, for a solid particle in a solidifying matrix:

$$\Delta F^{adh} = \gamma_{PS} - \gamma_{PL} - \gamma_{SL} \tag{5}$$

where γ_{PS}, γ_{PL}, and γ_{SL} are the interfacial tensions between, respectively, the particle and the solid epoxy, the particle and the liquid epoxy, and the solid and liquid phases of the epoxy. Using the equation of state approach to interfacial tensions [21], the interfacial tensions of Eq. (5) can be expressed in terms of the surface tensions of the particle, liquid and solid phase, γ_{PV}, γ_{LV}, and γ_{SV}, respectively. It can then be shown that ΔF^{adh} will be positive when $\gamma_{PV} < \gamma_{LV} < \gamma_{SV}$, indicating that the particles would be rejected by the advancing solid phase, since their inclusion would increase the free energy of the system [21]. Although we do not have the solid and liquid surface tensions of the present epoxy, previous contact angle measurements at 24°C on two other single-part heat-curing epoxies gave values of γ_{SV} and γ_{LV}, respectively, of 34 and 32 mJ/m^2 for one epoxy, and 39 and 27 mJ/m^2 for the other [22]. If it is further assumed that the surface tension of the hydrophobic silica particles is comparable with that of siliconized glass [21], about 18 mJ/m^2, then the above inequality in surface tensions would indeed be realized, supporting the possibility of this mechanism. This analysis shows only that the segregation of hydrophobic silica particles may be thermodynamically favored. It does not, however, address the speed with which such particles would move in the liquid resin and, hence, the rate of segregation. A procedure for assessing this has been developed for hydrophobic particles in a wide variety of organic melts [21].

If silica is being rejected by regions of solidifying epoxy, then one may also expect to see evidence of its localization in the bulk, since it is known that cure proceeds heterogeneously by the growth of dispersed "micro-gel" regions. Figure 4d shows an electron micrograph of the surface of ion-etched bulk epoxy. It is seen that there are indeed

numerous islands (1.3 – 3 μm) of relatively void-free resin, similar in appearance to the void-free region of the interphase shown in Figure 4c.

The observed interphase phenomena in the HYSOL EA9346 and A1-1100 epoxy-aluminum system give rise to many questions which warrant future investigation. For example, are the observed phenomena general or specific to the adhesive used in this study? What are the chemical and physical mechanisms involved? How is the interphase affected by such variables as surface pretreatment and cure cycle?

CONCLUSIONS

The interphase in an epoxy-aluminum system has been revealed and characterized using scanning electron microscopy, ion etching, energy-dispersive x-ray analysis, and nano-indentation. The interphase was of irregular thickness, nominally between 2 and 6 μm, and corresponded to a region of greater resistance to ion etching and a marked absence of the silica particles used in the epoxy adhesive. Nano-indentation tests, traversing the interphase from the aluminum to the bulk resin, showed that the interphase region had, on average, an effective elastic modulus, $E/(1-\nu^2)$, 13% greater than that of the bulk resin far from the aluminum. The interphase was also approximately 4% harder than the bulk adhesive.

Acknowledgements

The authors gratefully acknowledge the financial support of the Natural Sciences and Engineering Research Council of Canada and the scholarship program of the Ministry of Culture and Higher Education of Iran. We also thank Dr. B. Farahbakhsh, Dr. A. Rosenfeld and Mr. C. Pelow of Alcan International Ltd for their valuable advice and assistance with the nano-indentation tests.

References

[1] Cuthrell, R. E., *J. Appl. Polym. Sci.* **11**, 949 (1967).
[2] Hahn, O. and Koetting, G., *Welding and Cutting* **6**, E89 (1984).
[3] Knollman, G. C., *Int. J. Adhesion and Adhesives* **5**, 137 (1985).
[4] Williams, J. G., Donnellan, M. E., James, M. R. and Morris, W. L., *Mat. Res. Soc. Symp. Proc.* **170**, 285 (1990).

[5] Crompton, J. S., *J. Mat. Sci.* **24**, 1575 (1989).
[6] Skourlis, T. P. and McCullough, R. L., *Proc. Am. Soc. for Composites*, 218 (1994).
[7] Cognard, J., *J. Adhesion* **32**, 45 (1990).
[8] Maguire, J. F., Talley, P. L. and Lupkowski, M., *J. Adhesion* **45**, 269 (1994).
[9] Nakamae, K., Nishino, T., Airu, X. and Asaoka, S., *Int. J. Adhesion and Adhesives* **15**, 15 (1995).
[10] Affrosman, S., MacAllister, J. M. R., Pethrick, R. A., Thomson, B., Brown, N. M. D. and Meenan, B. J., *Polym. Surf. Interf.* **1**, 107 (1987).
[11] Wang, S. and Garton, A., *Proc. ACS Div. of Polym. Mater. Sci. and Eng.* **60**, 805 (1989).
[12] "Preparation of Metal Surfaces for Adhesive Bonding", ASTM D2651-79 Method G, American Society for Testing and Materials, Philadelphia, Pa. (1984).
[13] Oliver, W. C. and Pharr, G. M., *J. Mater. Res.* **7**, 1564 (1992).
[14] Doerner, M. F. and Nix, W. D., *J. Mater. Res.* **1**, 601 (1986).
[15] King, R. B., *Int. J. Solids Structures* **23**, 1657 (1987).
[16] Baker, S. P., *Proc. Mat. Res. Soc. Symp. Proc.* **308**, 209 (1993).
[17] Atkinson, M., *J. Mat. Sci.* **30**, 1728 (1995).
[18] Ramachandra Upadhaya, K. "Analysis of Thermodynamic Response for Materials Characterization Using Tensile and Nanoindentation Testing", PhD Thesis, Queen's University, Kingston, Ontario, p. 136 (1993).
[19] Pollack, H. M., Maugis, D. and Barquins, M., in *Microindentation Techniques in Materials Science and Engineering*, Balu, P. J. and Lawn, B. R., Eds., *ASTM STP 889* (American Society for Testing and Materials, Philadelphia), pp. 47–71.
[20] Baker, S. P. and Weihs, T. P., *Proc. Mat. Res. Symp. Proc.* **308**, 217 (1993).
[21] Li, D. and Neumann, A. W., in *Applied Surface Thermodynamics*, Neumann, A. W. and Spelt, J. K., Eds. (Marcel Dekker, New York, 1996), pp. 557 – 628.
[22] Unpublished data.